JMEPEG (2008) 17:714–724
DOI: 10.1007/s11665-007-9193-1

1059-9495/$19.00

Over-Aging Effect on Fracture Toughness of Beryllium Copper Alloy C17200

Kei-Peng Jen, Liqun Xu, Steven Hylinski, and Nate Gildersleeve

(Submitted May 8, 2007; in revised form December 8, 2007)

This study experimentally increased the fracture toughness of Beryllium Copper (CuBe) UNS C17200 alloy using three different age hardening processes. At the same time, the micro- and macro-fracture behavior of this alloy were comprehensively studied. ASTM E399 fracture toughness, tensile, and Charpy impact tests were conducted for all three heat-treated rods. The fracture surfaces were examined under both an optical microscope and a scanning electron microscope to investigate the failure mechanisms. Multiple test orientations were considered to explore isotropy. Increasing the temperature and duration at which age hardening was performed increased fracture toughness while decreasing ultimate tensile strength. The maximum fracture toughness was reached on the most overaged specimen, while retaining a serviceable tensile strength. The specimen test data allowed a relationship to be established among Charpy impact toughness, fracture toughness, and yield strength. Analysis of fracture behavior revealed an interesting relationship between fracture toughness and pre-cracking fatigue propagation rate.

Keywords electron microscopy, heat treating, mechanical testing, non-ferrous metals, optical microscopy

1. Introduction

UNS C17200 CuBe alloy is currently being used in drill collars and other components for down-hole energy exploration drilling rigs. CuBe alloy is well suited to these applications because of its resistance to galling, corrosion resistance, it is non-magnetic, and non-sparking (Ref 1, 5-7). Interests in CuBe alloy have increased dramatically in the past years because unlike most copper base alloys, which can only be work hardened, CuBe alloy can be age hardened to increase its fracture toughness (Ref 11-13).

When CuBe alloy is subject to high temperatures, Be is soluble in the copper matrix. However, at a low temperature, it forms a CuBe compound as the γ phase (Ref 8, 11). The Be may be retained in the Cu as a supersaturated solution by quenching the alloy from 800 °C, retaining good ductility and formability. Precipitation hardening takes place by re-heating above 205 °C, permitting the Be atoms to progressively react with Cu to form the γ phase. If this reaction is continued for the proper time the lattice strain which has occurred will produce maximum strength at room temperature (Ref 8). This can be achieved within 3 h at 315 °C.

During solidification of CuBe alloy, the amount of beta (β) phase should be as low as possible, since it is extremely hard and interferes with machining and forming operations. The β phase is unaffected by heat treatment. Well-dispersed, fine particles of β are not considered deleterious to material performance or properties. Overaging this alloy will increase the amount of γ phase in the grain boundaries, resulting in a lower tensile strength (Ref 13). When observed under a microscope after etching with ammonium persulfate/ammonium hydroxide, this γ phase appears dark along the grain boundaries (Ref 10, 11). For CuBe alloy, it is believed that overaging is a better approach to increase the fracture toughness than underaging.

The goal of this study is to analyze the effect of different age hardening temperatures and durations on increasing the fracture toughness of forged CuBe C17200 alloy. Three different aging temperatures and durations, discussed later in this article, are used in this study. In addition, the relationships among the fracture toughness, tensile strength, and Charpy impact toughness are investigated (Ref 12). It was desired to estimate the ASTM E399 fracture toughness from the tensile and Charpy tests, since they are easier and less expensive to conduct. The isotropy of fracture toughness behavior is carefully considered in this study.

After failure, the fracture surfaces of the fracture toughness specimens were studied using an optical microscope and a scanning electron microscope. The pre-cracking zones on the specimens made according to the ASTM E399 specifications provided additional opportunity to study the C17200s fatigue crack growth mechanisms.

2. Materials

The UNS C17200 in this study is treated in the order of solution treatment, water quenching, and age hardening. A 35.5 cm diameter wrought cylindrical C17200 bar was fabricated and solution treated. After solution treatment, four rods, designated R1, R2, R3, and R4 were sectioned from the cylindrical bar. All four rods were cut from the same hot-forged

Kei-Peng Jen, Liqun Xu, and **Steven Hylinski**, Villanova University, Villanova, PA 19085; and **Nate Gildersleeve**, NGK Metals Corporation, Sweetwater, TN. Contact e-mail: kei-peng.jen@villanova.edu.

Table 1 Heat treatments of beryllium copper alloy C17200

Material	Temperature, °C	Duration, h
R1	340	3
R2	390	6
R3	415	5
R4	445	5.5

bar. The sampled areas were taken from a relatively small region from a large production piece. The four rods are therefore considered equivalent to each other prior to heat treating. It was desired to heat treat the rods according to the parameters listed in Table 1. R1 was age hardened at 340 °C for 3 h for baseline performance evaluation. R2 was age hardened at 390 °C for 6 h, and R3 was age hardened at 415 °C for 5 h. R4 was reheated to 445 °C for 5.5 h. It was expected that the age hardening temperature and duration of R3 would produce the best combination of fracture toughness and strength for these overaged materials. The purpose of the reheated R4 was to confirm that R3 had achieved the optimized fracture toughness and strength.

An understanding of how the microstructure of CuBe alloy is affected by age hardening is important to make a well-informed decision on the optimum temperature and duration. Figures 1 to 3 show the microstructures of the R1, R2, and R3 materials at 200×. The microstructure of peak-aged R1 (Fig. 1) shows fine α grains with well defined γ phase along the grain boundaries. Dark fine CoBe beryllide particles are uniformly dispersed throughout the grains. Some larger CoBe particles are present inside of α grains. The flow lines caused by the forging process are elongated along the longitudinal direction of the forged cylinder.

When this material is overaged at higher temperature or for a longer period of time, more γ phase grain boundary precipitation develops. As shown in Fig. 2 and 3, the amount of grain boundary precipitation increases for overaged materials like R2 and R3. Grain boundary precipitation, by area, increases from 2-3% in Fig. 1, to 6-7% in Fig. 2, to 8-10% in Fig. 3.

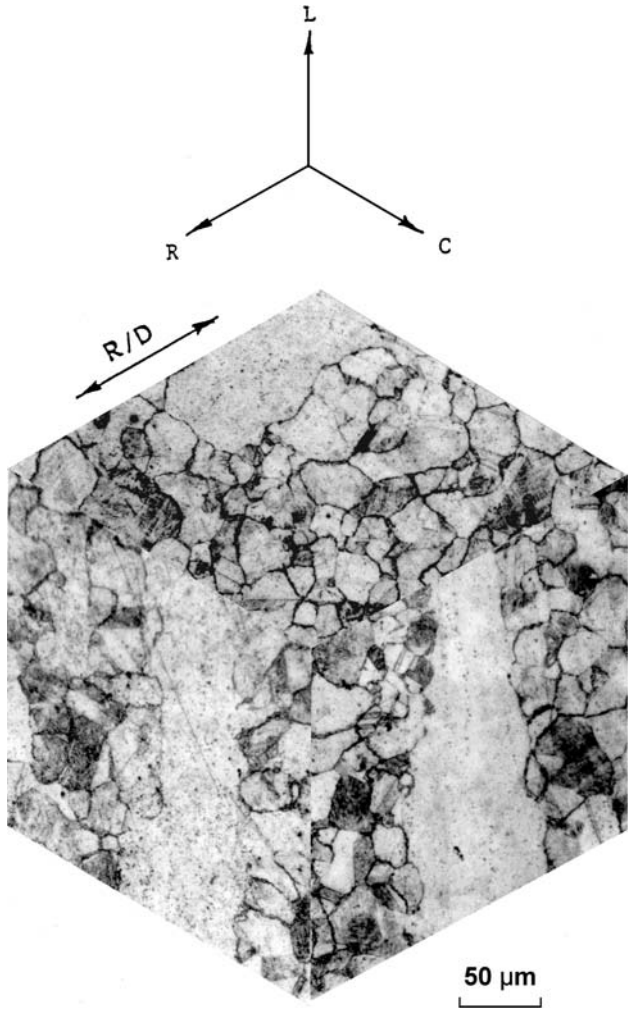

Fig. 1 3D microstructure of R1

3. Experimental Specifications

3.1 Tensile and Charpy

The tensile test was performed according to the ASTM E8 standard (Ref 2). The specimen diameter is 12.8 mm, and the gage length is 50.8 mm. The Charpy Impact Test was carried out to ASTM E23 standards for a Type-A specimen (Ref 3). The locations and orientations of specimens for tensile and Charpy tests are shown in Fig. 4. The Charpy impact and tensile tests were only performed in the longitudinal and transverse directions.

3.2 Fracture Toughness

3.2.1 Sample Orientations. In order to study the anisotropic behavior caused by the forging process, compact tension specimens were prepared for CR, RC, LC, and LR orientations, according to the ASTM E399 standard (Ref 4). These four orientations are most critical in the oil drilling industry. Figure 5 illustrates these orientations. The relationships among Charpy, tensile, and compact tension specimens should be noted. The transverse tensile orientation (Fig. 4) was treated as equivalent to the ASTM E399 CR or RC orientations, and the tensile longitudinal orientation considered equivalent to ASTM E399 LC or LR orientations. The transverse Charpy orientation (Fig. 4) is assumed to be similar to the ASTM E399 CR or RC, and the longitudinal Charpy similar to LC and LR orientations.

3.2.2 Experimental Setup and Fatigue Pre-Crack. The fracture toughness tests were conducted in accordance with the ASTM E399 compact tension test (Ref 4) guideline. For all specimens, $B = 1.52$ cm and $W = 3.05$ cm. A chevron starter notch was used for all specimens. A Sonntag model SF-1U fatigue-testing machine was used during the specimen pre-cracking. A cyclic load of 30 Hz was used to grow the fatigue pre-crack. The stress ratio was kept at 0.1 to provide one-way tension fatigue. During the pre-cracking, the reduction in P_{max} for step-down was no greater than the 20% value suggested by ASTM E399 (Ref 4).

A Fractomat® 1288 microprocessor, combined with Krak-Gages (Type CD-23-10A), was used to automate crack length measurement on the compact tension specimens (Ref 9). When the crack length reached a preset value of 0.55a/W, the Sonntag fatigue machine was stopped.

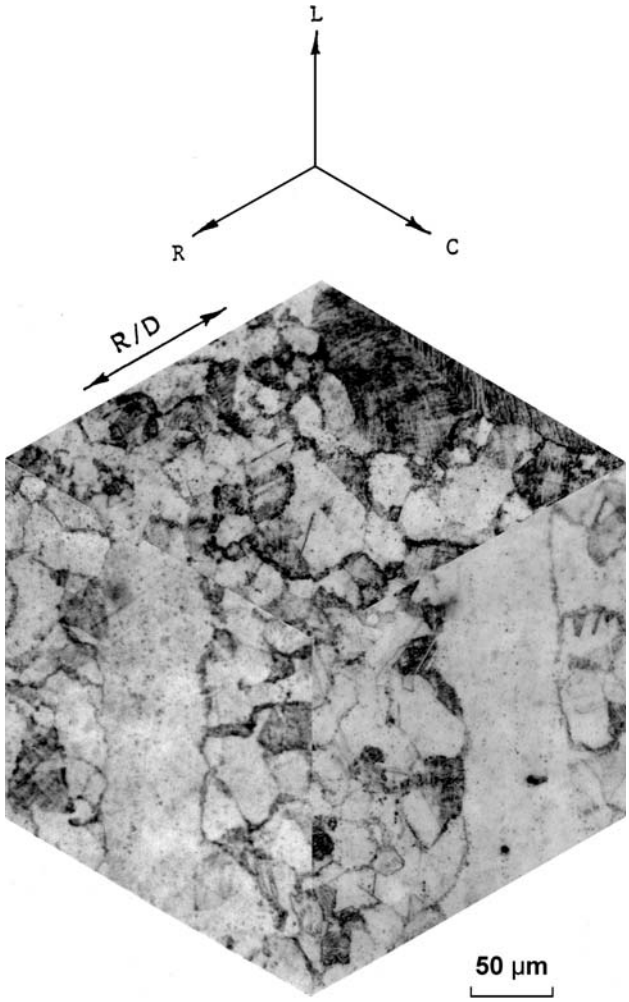

Fig. 2 3D microstructure of R2

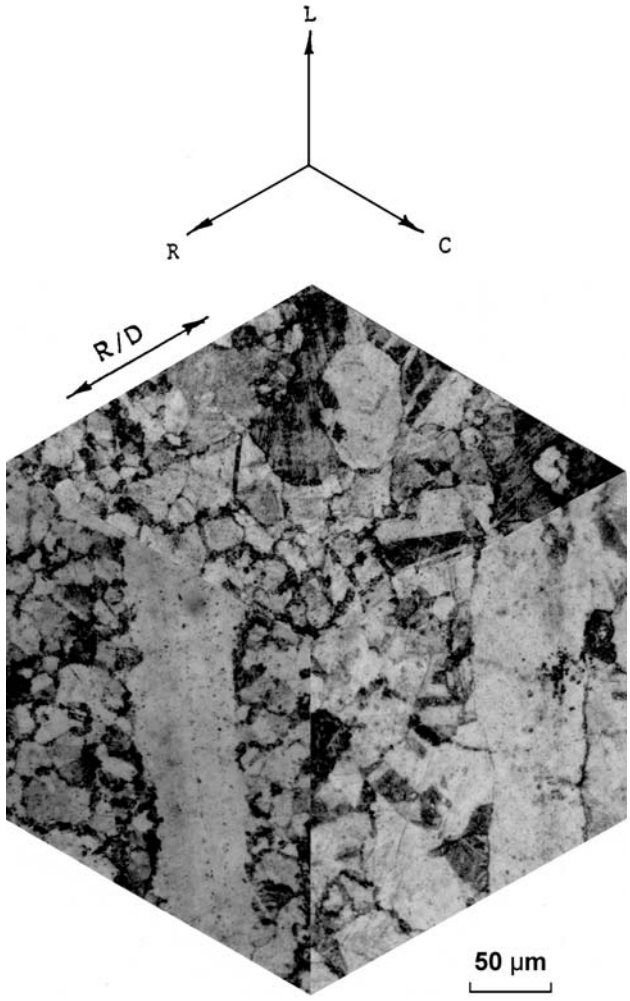

Fig. 3 3D microstructure of R3

After the pre-cracking, an INSTRON® 1125 Universal Testing Machine was used to load the pre-cracked specimens until fracture. All loadings-to-failure were conducted at 0.05 mm/min crosshead speed and 21 °C. A crack-opening-displacement (COD) gage was used to provide load versus COD output necessary to allow K_{IC} determination. Five fracture toughness specimens were tested for R1, R2, and R3 rods in each orientation.

4. Results and Discussion

4.1 Tensile Properties

Tensile properties including 0.2% offset yield strength, ultimate tensile strength, and elongation are listed in Table 2. Although the strengths are different for all three rods, no significant anisotropy exists in the tensile and yield strengths for each rod. As the overaging temperature and duration increased, tensile and yield strength decreased, while ductility increased. Due to the peak age treatment, R1 had the highest strength and lowest ductility.

4.2 Charpy Impact Toughness

Table 3 lists the Charpy V-Notch impact test data. The lateral expansion and percentage of shear fracture are also listed in the table. Charpy impact toughness increased as the overaging temperatures and durations were increased. Although the longitudinal orientation for each individual rod had a

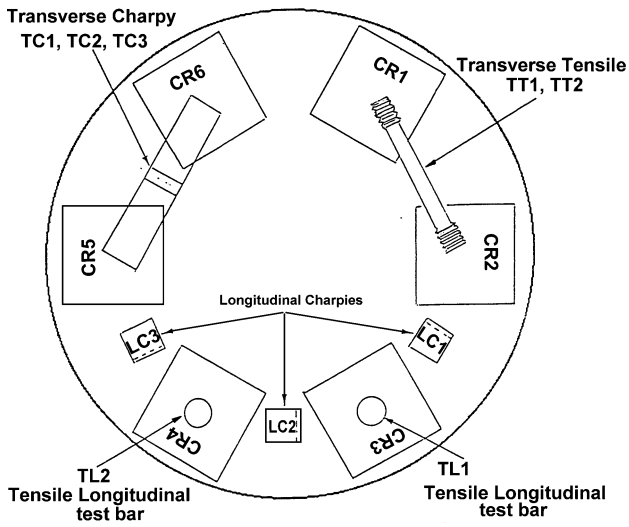

Fig. 4 Locations of 4 tensile specimens and 6 Charpy specimens

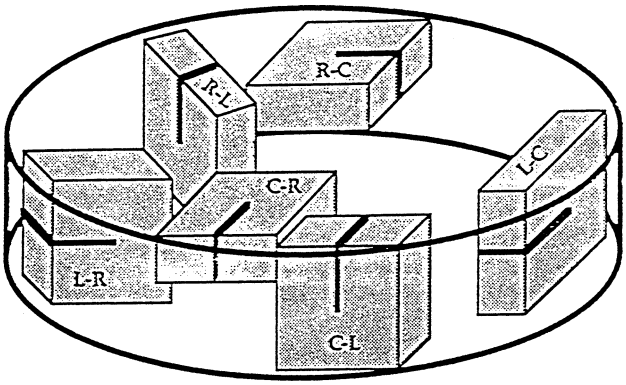

Fig. 5 ASTM notation for CT specimens extracted from cylinders

Table 2 Tensile test results for C17200

Specimen ID	Tensile strength, MPa	Yield strength (0.2 offset), MPa	Elongation, %	Reduction of area, %
A. Transverse tensile test data				
1TT1	1215	1077	2.7	3.2
1TT2	1204	1110	3.0	7.7
R1 TT Avg.	1209	1094	2.9	5.5
2TT1	958	818	9.6	23.2
2TT2	955	828	9.3	21.8
R2 TT Avg.	956	823	9.5	22.5
3TT1	871	699	14.2	27.5
3TT2	905	752	14.0	35.4
R3 TT Avg.	888	726	14.1	31.5
B. Longitudinal test data				
1TL1	1255	1085	6.6	10.8
1TL2	1251	1105	5.4	9.3
R1 TL Avg.	1253	1095	6.0	10.1
2TL1	990	818	13.0	26.7
2TL2	997	828	14.0	34.0
R2 TL Avg.	993	823	13.5	30.4
3TL1	843	665	16.6	35.0
3TL2	904	751	16.4	38.1
R3 TL Avg.	874	708	16.5	36.6

slightly higher average value than the transverse orientation, the difference was small. Charpy impact toughness increases with increasing ductility but decreases with the increasing tensile strength. R3 has the highest Charpy impact toughness values.

4.3 Fracture Toughness

Table 4 is the baseline fracture toughness test results from R1. Almost all the specimens satisfied the K_{IC} requirements including $P_{max}/P_q \leq 1.1$, $a,B \geq 2.5(Kq/YS)^2$, and $0.45 \leq a/W \leq 0.55$, etc. The K_{IC} fracture toughness increases in the order of RC, CR, LC, and LR orientations. The RC orientation has the lowest average K_Q value, 31.79 MPa-m$^{1/2}$, while the LR orientation has the highest K_{IC} value, 40.88 MPa-m$^{1/2}$. The increment is about 29% from the RC to LR orientations. Therefore, the anisotropic behavior of C17200 forged rod can be significant with respect to fracture toughness. The K_{IC} values of longitudinal directions (LC or LR) are higher than K_{IC} values of transverse directions (CR or RC).

Table 3 Charpy V-Notch impact test data for C17200

Specimen ID	*J*	Lat. Exp., mm	%Shear
A. Transverse Charpy (TC)			
1TC1	8.1	0.05	5
1TC2	8.1	0.10	5
1TC3	6.8	0.05	5
R1 TC Avg.	7.7	0.07	5
2TC1	13.6	0.10	15
2TC2	14.9	0.13	15
2TC3	13.6	0.10	15
R2 TC Avg.	14.0	0.11	15
3TC1	21.7	0.25	30
3TC2	23.0	0.25	30
3TC3	21.7	0.23	30
R3 TC Avg.	22.1	0.25	30
B. Longitudinal Charpy (LC)			
1TL1	8.1	0.08	5
1TL2	8.1	0.05	5
1TL3	8.1	0.08	5
R1 TL Avg.	8.1	0.07	5
2TL1	17.6	0.20	25
2TL2	17.6	0.15	25
2TL3	19.0	0.18	25
R2 TL Avg.	18.1	0.18	25
3TL1	31.2	0.36	35
3TL2	29.8	0.36	35
3TL3	28.5	0.38	35
R3 TL Avg.	29.8	0.36	35

Table 4 Fracture toughness of R1 material, MPa-m$^{1/2}$

Orientation	K_{IC}	STD
RC	31.8	1.64
CR	34.4	1.56
RC/CR Avg.	33.1	1.60
LC	37.7	1.20
LR	40.9	1.71
LC/LR Avg.	39.3	1.46

Table 5 Fracture toughness of R2 material, MPa-m$^{1/2}$

Orientation	Toughness K_{IC}	STD
RC	50.2	1.67
CR	51.1	3.59
RC/CR Avg.	50.6	2.63
LC	55.1	1.51
LR	56.3	1.36
LC/LR Avg.	55.7	1.43

Table 5 lists the summary of fracture toughness test results of R2. This material was intentionally overaged. It shows good improvement in fracture toughness over R1. The K_Q (not valid K_{IC}) fracture toughness increases in the same order of orientation as R1. The RC orientation has the lowest K_Q, 50.16 MPa-m$^{1/2}$. The LR orientation has the highest K_Q, 56.30 MPa-m$^{1/2}$. Clearly, the data indicates that anisotropic behavior still exists in this material but the degree of the anisotropy has been significantly reduced by overage hardening. In R2, the increment of fracture toughness from RC to LR

Table 6 Fracture toughness of R3 material, MPa-m$^{1/2}$

Orientation	Toughness K_Q	STD
RC	65.3	1.67
CR	66.2	1.44
RC/CR Avg.	65.7	1.55
LC	69.2	1.70
LR	69.1	1.47
LC/LR Avg.	69.1	1.59

Table 7 Fracture toughness of reheated material (R4), MPa-m$^{1/2}$

Orientation	Toughness K_Q	STD
3LC6.Rod3	70.3	0.42
3LR4.Rod3	70.2	
3LC2.Rod2	69.4	
Average	70.0	

direction is only 12%. The data indicates that RC and CR can be treated as one group while LC and LR can be treated as another group. When the toughness increases, the tensile and yield strengths decrease. Compared to R1, the tensile strength of R2 has dropped from 1231 to 975 MPa.

The results summary of R3 material is presented in Table 6. Although the overall K_Q fracture toughness for R3 in the LR/LC orientations is slightly higher than that in the RC/CR orientations, it is clear that the notable anisotropic behavior seen in the R1 fracture toughness data is almost eliminated. There are almost no fracture toughness differences between RC and CR orientations and LC and LR orientations. The RC orientation has the lowest K_Q, 65.25 MPa-m$^{1/2}$, while the LC orientation has the highest K_Q, 69.16 MPa-m$^{1/2}$. The fracture toughness increases about 6% from the transverse orientation to longitudinal orientation. Although the fracture toughness of R3 is the highest among R1, R2, and R3, the tensile strength (881 MPa) and yield strengths (717 MPa) are lower than R2. Compared with R2, the fracture toughness of R3 increases at least 10 MPa-m$^{1/2}$ for each orientation. The fracture toughness in LR/LC orientations increases about 22% while the RC/CR orientations increase about 30%.

Table 7 lists the results of the three reheated R4 specimens. These three specimens were reheated to 445 °C for 5.5 h from one of each of the R1, R2, and R3 rod samples. The reheating was used to verify that R3 had achieved the optimized fracture toughness and strength. The R4 specimens obtain an average K_Q value of 69.96 MPa-m$^{1/2}$. Although this value is slightly higher than that of longitudinal direction of R3, the sacrifice in the yield strength is substantial. From the hardness value of this specimen (R_c = 35), the yield strength was estimated to be near 586 MPa. The ductility of the reheated R4 material was so high that the requirements of P_{max}/P_q and thickness could not be satisfied; therefore K_{IC} could not be obtained.

On the basis of the R4 data, it can be concluded that any overaging beyond R3 process may slightly increase the fracture toughness at the undesirable expense of diminishing yield strength. The combination of 69.23 MPa-m$^{1/2}$ in fracture toughness and 717 MPa in yield strength found in R3 is the best result obtained from this study for both strength and fracture toughness of this C17200 alloy.

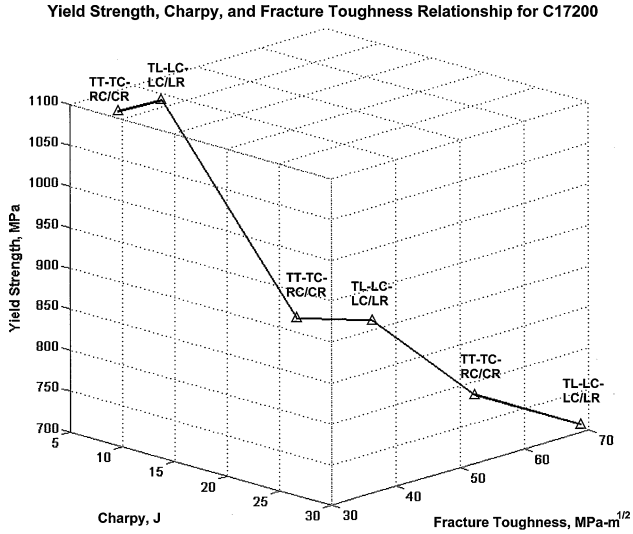

Fig. 6 3D curve of fracture toughness, Charpy toughness, and yield strength for C17200

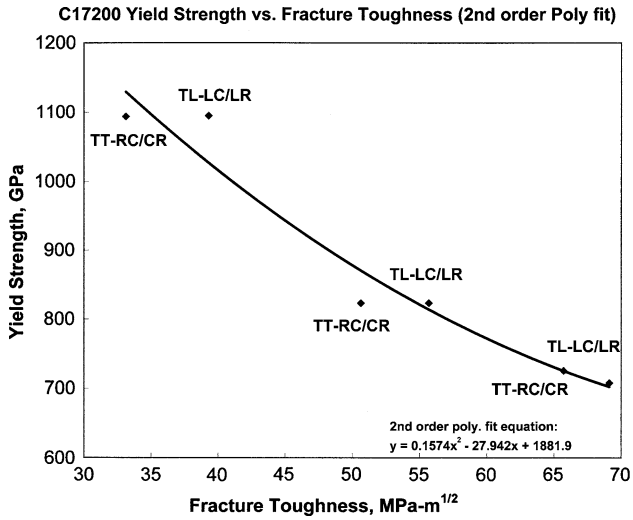

Fig. 7 Yield strength vs. fracture toughness of C17200 with polynomial fit

4.4 Relationship Among Yield Strength, Charpy, and Fracture Toughness

The relations among tensile strength, Charpy V-notch impact toughness and fracture toughness can be shown as a 3D curve in Fig. 6. Since, the orientations used in this study to prepare fracture toughness, Charpy, and tensile test specimens are not exactly the same, the relationships among yield strength, Charpy, and fracture toughness must built upon the closest orientations. Tension specimens have TT and TL designations while Charpy specimens have TC and LC designations. However, fracture toughness specimens have four designations, namely CR, RC, LC, and LR. In order to reduce the fracture toughness data to two orientations similar to tensile and Charpy tests, the average of CR and RC is treated as one group while the average of LC and LR is treated as another group. In Fig. 6, there are six data points on a 3D plot. Ideally, two curves can be constructed on this 3D plot to provide the

relationship among the tension, Charpy, and fracture toughness. One curve is based on TT-TC-CR/RC data and the other one is based on TL-LC-LR/LC data. However, Fig. 6 presents only a line connecting these six data points since it is hard to show two curves in a 3D plot.

It is desirable to estimate fracture toughness from yield strength and Charpy toughness in a 2D plot. They are shown in Fig. 7 and 8 with polynomial curve fitting. Note that these curves are plotted by using six points, including both longitudinal and transverse orientations. For design purposes, if the designation of CuBe specimens is not available, these curves can be referenced to estimate fracture toughness data by using yield strength data or Charpy V-notch impact data. For longitudinal orientation, the estimated fracture toughness by using all six points may be slightly lower than the actual value. Meanwhile, in the transverse direction, the estimated value may be slightly higher than actual.

4.5 Fracture Surface Analysis

Both the pre-crack and final fracture surfaces of the compact tension specimens were analyzed. The specimens were first observed at the macro scale, and then observed using an SEM. Generally speaking, the fracture surfaces of the CR and RC specimens were much rougher than the LC/LR specimens. The CR/RC pre-crack regions showed many shiny lines, whereas the LC/LR specimens had shiny specks in the pre-cracking region. These shiny specks and lines were the results of flow lines caused by the forging process, cut by the crack front during the pre-crack. Figure 9 is a photograph showing some examples of both shiny lines and specks in the pre-cracking regions of R1, R2, and R3. The abundance of shiny surface area increases in the order of R1, R2, and R3. Figure 10 shows a direct comparison between the shines of R1 and R3. It can be concluded that the more shiny area (including specks or lines) in the pre-cracking region, the higher the fracture toughness.

Interestingly, the fatigue pre-crack regions of R1 and R2 contained many dark spots. Figure 11 shows these dark spots on R1. R2 material had fewer dark spots than R1. However, R3

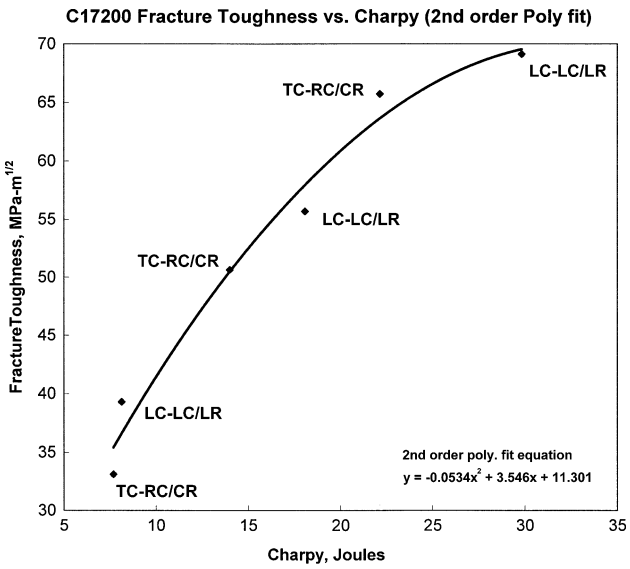

Fig. 8 Fracture toughness vs. Charpy of C17200 with polynomial fit

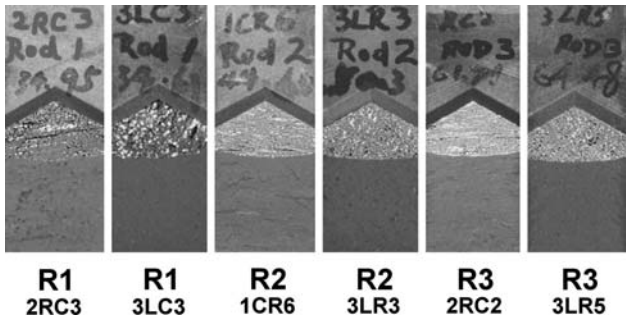

Fig. 9 Examples of shiny lines and shiny spots in fatigue regions of R1, R2, R3

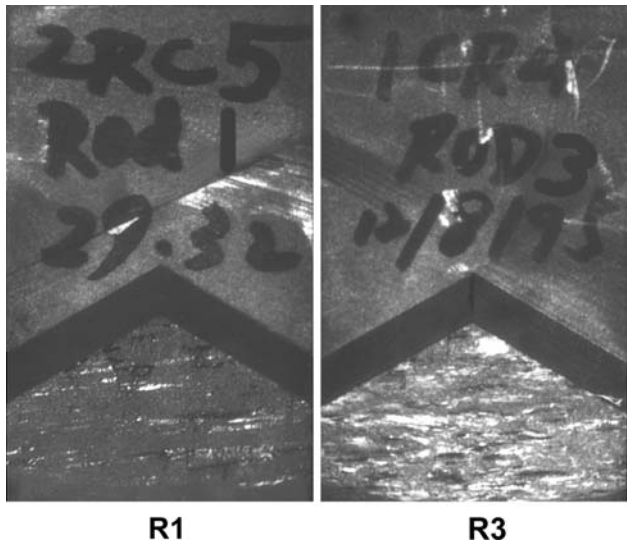

Fig. 10 Comparison of shiny areas of R1 and R3

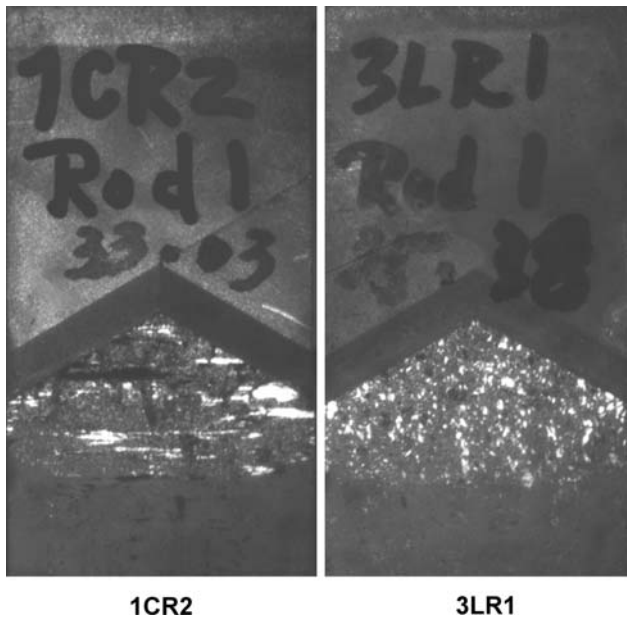

Fig. 11 Dark spots in fatigue pre-crack region of R1

had no dark spots at all. These dark spots are attributed to fretting oxidation caused by the rubbing actions between the top and bottom fracture surfaces. The rubbing effect was higher in RC and CR specimens than in LC and LR specimens due to their higher surface roughness.

Due to the similarity on the fracture surfaces, RC and CR orientations will be presented as one group for the following discussions, while LC and LR orientations are treated as another group.

4.5.1 CR/RC Orientations for R1 Material. Figure 12 reveals extensive cleavages along certain crystallographic planes in the shiny-appearing region mentioned above. It is one of the brittle fracture features in crystalline materials. In the pre-crack region, the R1 RC/CR specimens were quite rough, resulting in black oxidation dots from the rubbing effect. No fatigue striations could be found in the pre-crack region. The presence of cleavages in the fatigue pre-crack region indicates that the crack propagates in a brittle manner during fatigue.

In the overloaded region, R1 was characterized by intergranular dimples (Ref 11) and quasi-cleavages as shown in Fig. 13 and 14 (2RC5.R1). In this overloaded region, the amount of dimples in R1 was the least among all three rods. Therefore, the R1 material has the lowest fracture toughness due to its more quasi-cleavages and less dimple fractures in the overloaded region.

4.5.2 LC/LR Orientations of R1 Material. In the pre-crack region, the shiny regions mentioned above were dominated by river patterns (see Fig. 15). Some equiaxed dimples were also observed. In the overloaded regions (see Fig. 16), the intergranular dimples dominate the whole fracture surface and many cracks are found along the grain boundaries (Ref 11).

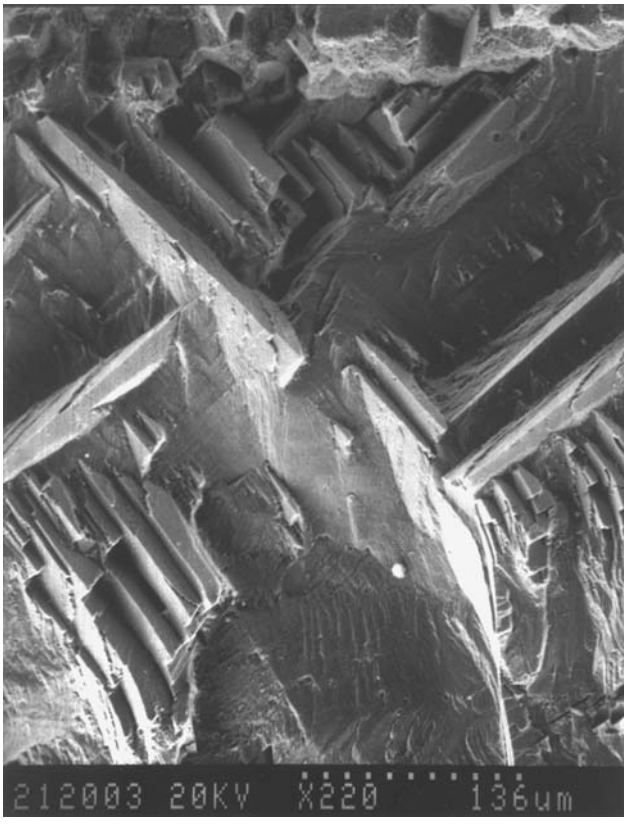

Fig. 12 Cleavages in R1 pre-crack region, RC orientation (220×)

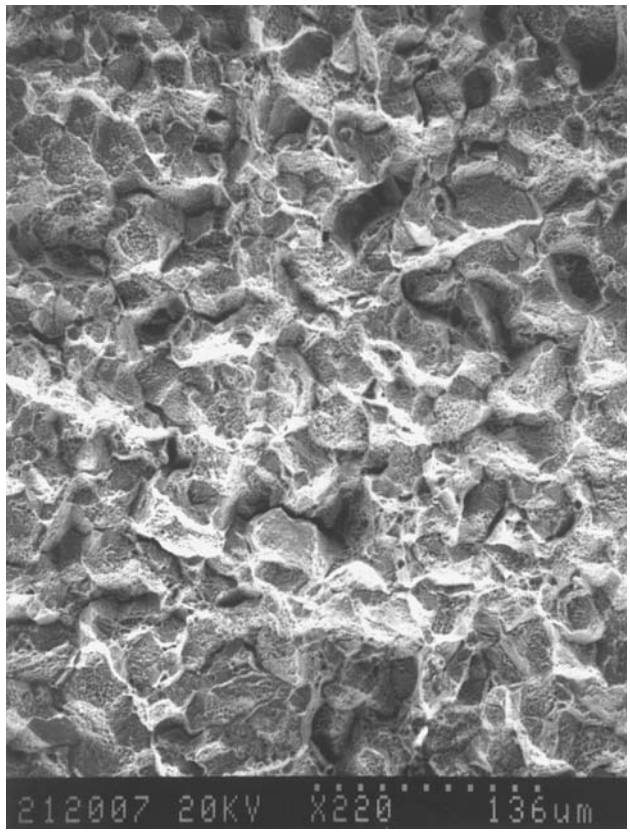

Fig. 13 Dimples and cleavages in R1 fracture region, RC orientation (220×)

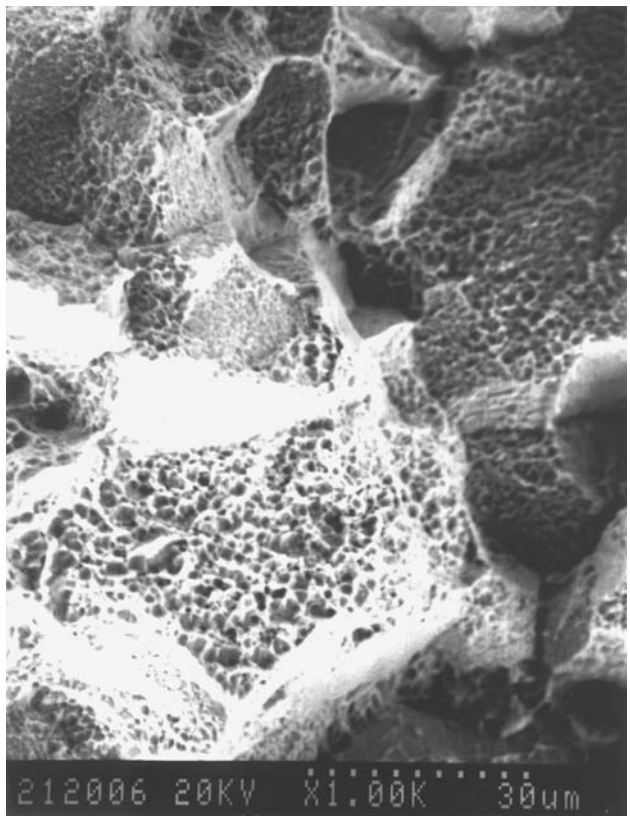

Fig. 14 Details of dimples and quasi-cleavages in R1 fracture region, RC orientation (1000×)

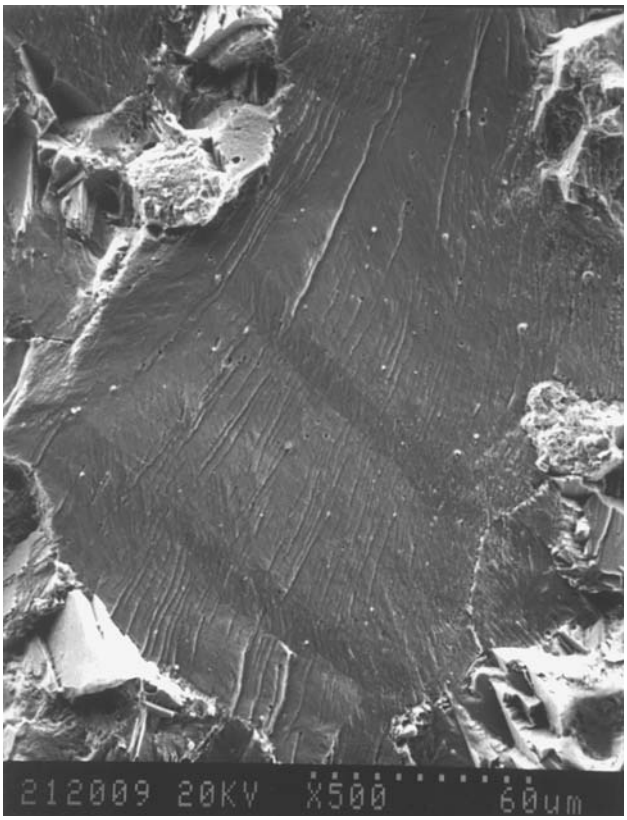

Fig. 15 River pattern in R1 pre-crack region, LR orientation (500×)

Fig. 16 Dimples in R1 fracture region, LR orientation (500×)

Fig. 17 Black dots in R1 pre-crack region, LC orientation (150×)

Figure 17 is a micrograph near a dark speck. The fracture surface is covered by the crushed debris caused by the rubbing effect on the rough surfaces (white area at the center of this photo).

The fracture surfaces of R2 and R3 were similar to each other since both rods were overaged. Therefore, they will be discussed together.

4.5.3 CR/RC Orientations for R2 and R3 Material. Similar to R1, R2, and R3 also showed many shiny lines across the fatigue pre-crack region. However, the pre-crack region of R2 and R3 looked completely different from R1 since they were dominated by the numerous river patterns instead of cleavages; see Fig. 18 and 12 for comparison. The river patterns, indicating brittle fracture, suggested that the fatigue crack may propagate at a considerably fast rate in R2 and R3 material. Interestingly, R3 had more river patterns than R2. This implies that R3 should have a faster fatigue crack propagation rate than R2 material under the same fatigue loading. Notice that Rod 3 has a higher fracture toughness than Rod 2. It seemed that for overaged C17200 alloy, it may have higher fracture toughness and faster fatigue crack propagation rate at the same time. Future work should include the ASTM E647 fatigue crack growth rate tests to further explore this observation.

Unlike the intergranular dimples dominating the overloaded region of R1, transgranular dimples dominated the whole surface of R2 and R3; see Fig. 19. Very few cleavages were found in the overloaded region of R2 and R3. R3 material contains many dimples with secondary cracks; see Fig. 20. The formation of secondary cracks would absorb fracture energy thereby promoting the highest fracture toughness in R3 material.

Fig. 18 River pattern in R2 pre-crack region, CR orientation (600×)

Fig. 19 Transgranular dimples with some cleavages in R2 pre-crack region, CR orientation (500×)

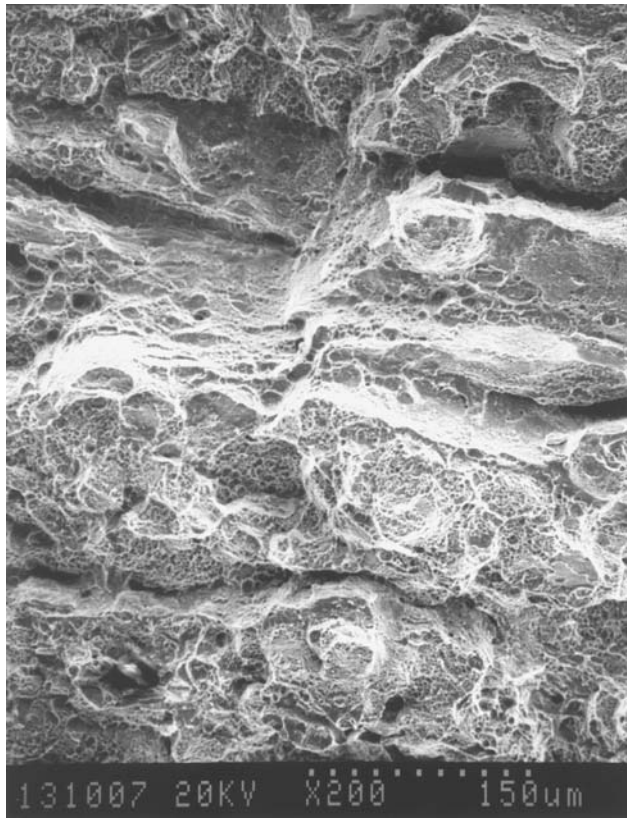

Fig. 20 Dimples in R3 fracture region, RC orientation (200×)

4.5.4 LC/LR Orientations For R2 and R3 Material. Similar to R1 material, R2 and R3 also showed many shiny specks on the fatigue fracture surface. All of the shiny specks displayed river patterns; see Fig. 21. For R3 samples, no cleavages were found in the pre-cracking region at all.

Figure 22 shows many dimples in the overloaded region. As shown in this figure, there are gaps between grain boundaries indicating ductility in this material. Overall, there were no fatigue striations seen in the fatigue region for all of the specimens.

5. Conclusions and Recommendations

5.1 Conclusions

1. For C17200 alloy, the peak-aged baseline material R1 achieves the highest fracture toughness of 40.88 MPa-$m^{1/2}$ in the LR direction. The highest fracture toughness, 68.13 MPa-$m^{1/2}$ in the LR direction, was reached by overaging R3 at 415 °C for five hours. The fracture toughness and yield strength values obtained from the R4 reheated specimens confirmed that the R3 yields the best combination of fracture toughness and strength, by overaging heat treatment for the C17200 alloy.
2. Test results indicate anisotropic fracture toughness behavior exists to various degrees, depending on thermal treatment. The anisotropy may be attributable to the relatively low hot working reduction ratio (original area to final area), which was approximately 8:1. This is further evidenced in the microstructure as seen in Fig. 1-3. In

Fig. 21 River patterns in R2 pre-crack region, LR orientation (400×)

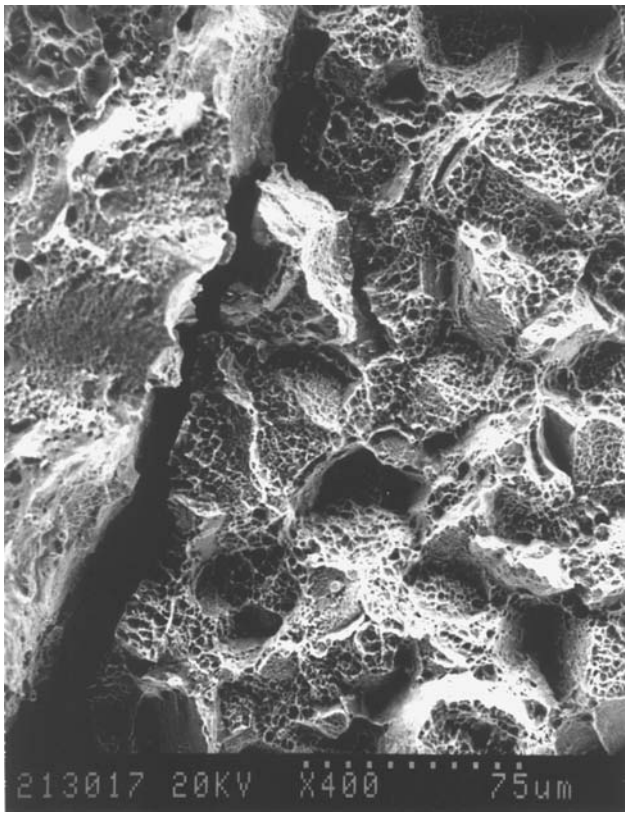

Fig. 22 R2 fracture region, LR orientation (400×)

general, the fracture toughness increases in the order of RC, CR, LC, and LR orientations. The LR orientation offers the maximum fracture toughness. This phenomenon is most significant in the peak-aged material. Overaging at higher temperature for a longer time causes the material to approach isotropic fracture toughness behavior. Overaging at 415 °C for five hours nearly removes all of the anisotropic effect in the fracture toughness data. Industrial application of this material takes appropriate advantage of the higher toughness performance in the longitudinal orientations. An environment of heavy axial loading, combined with sudden accumulation of axial and torsional stress place considerable emphasis on the materials ability to arrest rapid crack propagation in the LC and LR directions.

3. All three rods show ductile fracture (dimples) in the overloaded region. R1 is dominated by intergranular dimples while R2 and R3 display transgranular dimples.
4. In the fatigue region, the fracture surface contains many shiny lines (CR/RC specimens) or dots (LC/LR specimens) as a result of the crack propagating through the flow lines produced by forging process. For a specific rod, it was found that a specimen with a larger total area of the flow lines in the pre-cracking region possesses higher fracture toughness.
5. In the fatigue region, the crack tends to form river patterns in the shiny area, which indicates that the crack may propagate very fast in the flow line areas. Increasing size and abundance of flow lines seems to simultaneously increase the fracture toughness and fatigue crack growth rate for overaged material. Further investigation by conducting ASTM-E647 tests are required to verify this observation.
6. In the fatigue pre-crack region, the fracture surfaces of R1 material were significantly rougher than other rods and they revealed many dark spots. The dark spots were fretting oxidation caused by the rubbing effect on the rough surfaces.
7. Relationships among the fracture toughness, yield strength, and Charpy impact toughness were established. If fracture toughness test is not available, the fracture toughness value of C17200 can be estimated from the yield strength or Charpy impact toughness. Increasing the yielding strength will decrease the fracture toughness. Charpy impact toughness has a very good agreement with the fracture toughness.

Acknowledgment

The support of NGK Metals Corporation to the Mechanical Engineering Department of Villanova University is greatly acknowledged.

References

1. *Beryllium Copper Rod, Bar, Tube Products*, NGK Metals Corporation, April 2000
2. Standard Test Methods for Tension Testing of Metallic Materials, E8–87, *Annual Book of ASTM Standards*, ASTM, 2002, Vol 3.01, p 60–81
3. Standard Test Methods for Notched Bar Impact Testing of Metallic Material, E23–96, *Annual Book of ASTM Standards*, ASTM, 1996, Vol 3.01, p 136

4. Standard Test Method for Plane-Strain Fracture Toughness of Metallic Materials, E399–90, *Annual Book of ASTM Standards*, ASTM, 1996, Vol 3.01, p 407
5. D.W. Crossley and E.M. Foster, Beryllium Copper & its Applications, *Telegraph Constr. Maint.*, January 1943, **20**
6. F. Dunlevey, Performance of a Beryllium Copper Nonmagnetic Drill Collar Alloy, *SPE*, December 01, 1986
7. R.G. Forman and J.A. Henkener, An Evaluation of the Fatigue Crack Growth and Fracture Toughness Properties of Beryllium-Copper Alloy CDA172, *NASA Technical Memorandum 102166*, September 1990
8. L.M. Halleran, Beryllium Copper Part II: An Alloy Well-Suited for Today's Trend Toward Increased Production Speeds and Decreased Product Size, *Springs*, 1998, **37**(3), p 75–79 Summer
9. P.K. Liaw, W.A. Logsdon, L.D. Roth, and H.R. Hartmann, Krak-gages for Automated Fatigue Crack Growth Rate Testing: A Review, *Automated Test Methods for Fracture and Fatigue Crack Growth*, ASTM STP 877, 1985, p 177–196
10. K.E. Noll, Experimental Heat Treatment of Beryllium Copper Alloy, *NTIS*, May 1994
11. K.V. Sudhakar, J.C. Cisneros, H. Cervantes, and C.G. Pineda, *Machining Characteristics and Fracture Morphologies in a Copper-Beryllium Alloy*, ASM, February 2006, Vol 15 (Issue 1), p 117–121
12. M.G. Ultichny, Aging Study of Copper Alloy 172. Final Report, *NTIS*, April 01 1985
13. K.G. Wikle, Beryllium Copper: An Overview of Heat Treat Techniques, *Heat Treating*, 1981, **13**(34), p 28–31